Applied Catalysis A, General 559 (2018) 187–194

Contents lists available at ScienceDirect

Applied Catalysis A, General

journal homepage: www.elsevier.com/locate/apcata

Diversity of Pd-Cu active sites supported on pristine carbon nanotubes in terms of water denitration structure sensitivity

Sanja Panic[a,*], Vladimir Srdić[a], Tamás Varga[b], Zoltán Kónya[b,c], Ákos Kukovecz[b], Goran Boskovic[a]

[a] University of Novi Sad, Faculty of Technology, bul. Cara Lazara 1, 21000 Novi Sad, Serbia
[b] Department of Applied and Environmental Chemistry, University of Szeged, Rerrich Bela ter 1., 6720 Szeged, Hungary
[c] MTA-SZTE Reaction Kinetics and Surface Chemistry Research Group, Rerrich Bela ter 1., 6720 Szeged, Hungary

ARTICLE INFO

Keywords:
Pd-Cu/CNTs catalysts
Water denitration
Pd Particle size
Bimetallic particle composition
CNT lattice defects
Structure sensitivity effect

ABSTRACT

Four Pd-Cu-based (2:1 wt.%) catalysts for water denitration, differing in physico-chemical characteristics and structural quality, were prepared, using carbon nanotubes (CNTs) as supports. The extent of lattice defects in the pristine CNTs turned out to govern resulting varieties of Pd nanoparticle size and the composition of the bi-metallic (Pd:Cu) entities in the catalysts, playing an important role in nitrate reduction. Catalyst samples characterized by close proximity of Pd and Cu, as in an alloy, displayed the highest degree of nitrate conversion. At the same time, the size of the Pd particles, alone, or decorated to different extents with Cu atoms, was found to be critical for the second step of denitration reaction, directing the formed nitrite to either N_2 or NH_3. Water denitration is a structure sensitive reaction related to Pd particle size, and this effect is further emphasized in the decoration of the particle by the incorporation of Cu atoms into Pd particle corners and edges.

1. Introduction

The global drive towards sustainability requires ongoing scientific efforts in all aspects of modern society, including the production of safe drugs, renewable fuels, new materials and environmental protection. Transitioning from noncatalytic to catalytic reactions is one way in which chemical processes might come to justify the label sustainable [1]; and the synthesis of new efficient catalysts is the essence of such research. Nanosized catalysts have become a focus of interest because it is possible to tailor the size and shape of metal nanoparticles, and consequently alter catalyst performance and adjust it to various applications. The preparation of appropriate nanocatalysts requires the selection of supports that enable the maximum dispersion and stability of metal nanoparticles on their surfaces. The most common supports used for the deposition of mono- or bi-metallic active phases are oxides, zeolites and different types of carbon materials [2]. The use of carbon nanotubes (CNTs) as catalyst supporting materials started not long after their discovery in 1991. It has been reported that both single and multiwalled CNTs are highly effective in stabilizing small metal clusters and creating catalysts with improved activity [3]. The strong metal-anchoring ability of nanotubes has been recognized as the mechanism enabling uniform deposition of metal nanoparticles [4]. Different types of defects and functional groups attached to CNT surfaces have been proposed as the main anchoring sites for metal nanoparticles [5,6]. Many authors agree that greater numbers of oxygen surface functional groups facilitate higher metal dispersion. On the other hand, there is the opinion that functional groups are not the anchoring sites for metal particles, but rather contribute to a better wetting, and therefore a better dispersion in the aqueous metal precursor phase [7,8].

CNT-based nanocatalysts have already been utilized in numerous reactions, the majority of them having environmental significance. The presence of nitrates in surface and ground water due to fertilizer abuse is a major environmental issue, as nitrate ions are potentially harmful to human health. The European Commission has established maximum allowable concentrations in drinking water for nitrates (50 ppm), as well as for nitrites (0.5 ppm) and ammonium (0.5 ppm) as their respective intermediates and by-products [9]. Although biological and physico-chemical methods for nitrate removal have been developed, catalytic denitration is still under study because of its economic and ecological benefits [10–12]. Since the pioneering work of Vorlop and Tacke in 1989 [13], various bimetallic catalytic systems, consisting of a precious metal (Pd, Pt and Rh) and a promoting transition metal (Cu, Ni, Fe, Sn and In), have been widely tested with the aim of discovering a highly efficient active phase with satisfactory activity and nitrite and ammonium selectivity. Among them, the Pd-Cu active phase has been highlighted in many reports as the most effective system, but as still inadequate in terms of its selectivity to nitrogen [14,15]. The catalytic reduction of nitrate is generally accepted to be a stepwise reaction. The

* Corresponding author at: Faculty of Technology, University of Novi Sad, Bulevar cara Lazara 1, Novi Sad, Serbia.
E-mail address: sanjar@tf.uns.ac.rs (S. Panic).

https://doi.org/10.1016/j.apcata.2018.04.032
Received 14 March 2018; Received in revised form 17 April 2018; Accepted 24 April 2018
Available online 25 April 2018
0926-860X/

presence of Cu in the catalyst allows the conversion of nitrate to nitrite, while the further reduction of nitrite to nitrogen or ammonium occurs mainly on Pd active sites [16–18]. Besides being characterized by a high potential for hydrogen chemisorption, Pd has a pronounced effect of hydrogen spillover on Cu, enabling its regeneration, and consequently the conversion of nitrate to nitrite. Therefore, it is essential that these two metals are in close contact, which can be achieved either by applying an appropriate preparation method (Pd/Cu atomic ratio) or using a suitable catalyst support [19–21].

In the present work, four bimetallic (Pd-Cu) catalysts supported on pristine CNTs of different structural quality were used in the liquid-phase catalytic reduction of nitrate. According to the literature review, in most of the research studies dealing with CNT-based catalysts the functionalization of the tubes was a prerequisite step in the catalyst preparation procedure. The application of chemically unmodified tubes has not received sufficient attention regardless of their initially different structural properties. That is to say, functionalization processes, requiring the application of strong acids, may be understood as substitutes for the formation of anchoring sites, (i.e. defects), by means of tube preparation procedures using various catalysts. In this regard, the aim of this work was to synthesize Pd-Cu nanocatalysts using pristine CNTs of different structural quality, evaluate the influence of their surface chemistry on the metal active phase characteristics, and then test the performances of the prepared catalysts in water denitration reactions. The dependence of catalytic performance on the size and chemical composition of metal nanoparticles was also examined, emphasizing their impact on nitrite and ammonium selectivity.

2. Experimental

2.1. Synthesis of bimetallic Pd-Cu catalysts with MWCNTs as a support

The bimetallic Pd-Cu/CNT catalysts used in the study were synthesized at room temperature by wet coimpregnation from aqueous solutions of the corresponding metal precursors, $PdCl_2$ (Alfa Aesar GmbH & CoKG, Germany) and $Cu(NO_3)_2{\cdot}3H_2O$ (Centrohem, Serbia), aiming at nominal concentrations of 2 wt.% Pd and 1 wt.% Cu on related CNTs. The catalyst suspensions obtained were treated in an ultrasonic bath for 3 h, followed by vacuum evaporation in a rotary vapour apparatus, and overnight drying at 110 °C. The Pd-Cu/CNT catalysts were heat treated for 1 h in a nitrogen flow (110 ml/min) at 250 °C and then reduced at 150 °C for 3 h in a hydrogen flow (110 ml/min). The heat treatment in a nitrogen flow was selected in order to completely preserve the structure of the CNTs, while the selection of the appropriate temperatures was supported by the well known high potential of Pd for hydrogen chemisorption even at lower temperatures. Also, the reduction of the formed Cu oxides is usually promoted by the presence of Pd, lowering the required reduction temperature of the bimetallic catalysts compared to the pure CuO, as well as the supported monometallic one [22,23]. The similar conditions for the heat treatment of Pd-Cu/CNT catalysts can be found in the literature [24,25]. EDS analysis was performed to examine the metals present in the catalyst samples, both qualitatively and quantitatively. The results of the elemental analysis indicated that the catalyst samples had both metals loading close to their nominal values (Table 1).

Multi-walled carbon nanotubes (MWCNTs) used as supports for the preparation of bimetallic Pd-Cu catalysts for water denitration had been synthesized previously [26]. Briefly, the synthesis of the MWCNTs was carried out in a home-made reactor setup, at 700 °C, using ethylene as the carbon source [27,28], and four different catalysts having either Co or Mo next to Fe in the active phase, supported on Al_2O_3 or MgO. All four MWCNT products, purified of catalyst remains, represent dense networks without any traces of amorphous carbon and catalyst remains [26]. Their morphological, textural and structural properties, as represented by the extent of their lattice defects, and their different structures and dispersion, depended primarily on the catalyst used. Thus, the nanotubes synthesized over MgO-supported catalysts were characterized by narrower outer diameter distribution profiles, compared to their Al_2O_3-originated counterparts. Likewise, higher values of specific surface area and pore volume, as well as lower values of pore diameter, were found in Al_2O_3-originated nanotubes. Crystalline quality and inclination to defect points formation in the growing nanotubes were dependent on the character of the second metal sitting next to Fe. Thus the presence of Co in the active phase resulted in CNTs with a high number of lattice defects, reaching the highest defect density in the CNT series for the Al_2O_3-originated nanotubes. Molybdenum, however, results in the production of nanotubes with entirely different crystalline qualities regardless of the catalyst support (Alumina or M-agnesia) used. Mo stabilizes Fe, enabling the growth of CNTs with no, or minor numbers of lattice defects. Likewise, Mo has a positive influence on multilayer graphitic structure, preventing its deterioration. The effect was enhanced when magnesia was used as the catalyst support (Table 1) [26].

As the Pd/Cu loading was equal for all the synthesized denitration catalysts, and they differed only in the properties of their applied supports (CNTs), the labeling procedure follows the preparation history of the corresponding CNTs, including their supports (A or M) and the second metal (Co or Mo) present in the Fe-active phase of their grown-catalysts: Pd-Cu/CNT_{ACo}, Pd-Cu/CNT_{AMo}, Pd-Cu/CNT_{MCo} and Pd-Cu/CNT_{MMo} (Table 1).

2.2. Test reaction – catalytic denitration

Catalyst performances were tested for denitration reaction in a water model system, in a semi-batch reactor equipped with a magnetic stirrer [29]. The applied experimental conditions are shown in Table 2.

The test reaction procedure was performed as follows:

The previously reduced catalyst, weighing 300 mg, was fed into the reactor containing the prescribed volume of demineralized water, under constant stirring. In order to remove the oxygen present, nitrogen (110 ml/min) was passed through the reaction mixture for 15 min, followed by a gaseous mixture of hydrogen and carbon-dioxide (220 ml/min flow rate, 1:1) saturation for 30 min, the CO_2 acting as a pH buffer (pH = 6). Subsequently, an appropriate volume of $NaNO_3$ (Centrohem, Serbia) solution was added to the catalyst-water suspension in order to achieve an initial NO_3 concentration equal to 100 ppm, this indicating zero time for the reaction. Samples from the reactor were taken at defined time periods, in a careful manner, to avoid extracting catalyst particles. Although, this kind of sampling procedure does not ensure the preservation of the catalyst loading, it can be assumed that the loading is only slightly changed due to a very small volume of the taken samples in relation to the water model system volume. Nitrate, nitrite and ammonium concentrations were assessed by UV-VIS spectrophotometry (Cecil Instruments 2021), and also using Lovibond ChecKit reagents (Tintometer GmbH, Germany) for colour change chemical reactions.

2.3. Characterization of Pd-Cu/CNT catalysts

The morphology of Pd-Cu/CNT denitration catalysts was examined by transmission electron microscopy (FEI TECNAI G2 20X-TWIN Transmission Electron Microscope) (TEM). X-ray diffraction (XRD) measurements were performed on a Rigaku Miniflex 600 (CuKα radiation $\lambda = 0.15406$ nm) using a counting step of 0.3° and a counting time per step of 3 s. The average diameters of crystallites were derived using the Scherrer equation. Raman spectra of the samples were obtained using a DXR Raman Microscope with a diode-pumped solid state laser (DPSS), wavelength $\lambda = 532$ nm. The laser was coupled with CCD camera as a detector, full range grating (900 lines/mm), 10x microscope objectives and OMNIC software for collecting and analyzing the spectra. All the samples were exposed to the radiation of the laser with power of 9 mW, six times for 30 s.

Table 1
CNT support properties, phases structures and metal particle sizes for the Pd-Cu/CNT catalyst samples for water denitration.

Catalyst samples					
Properties		Pd-Cu/CNT_{ACo}	Pd-Cu/CNT_{MCo}	Pd-Cu/CNT_{AMo}	Pd-Cu/CNT_{MMo}
CNT properties		High degree of lattice defects	High degree of lattice defects	Low degree of lattice defects	Minor lattice defects
Average particle size by TEM, nm (dispersion, %)		14 (7.7)	15 (7.2)	20 (5.4)	13 (8.3)
Pd (Cu) loading by EDS, wt.%		2.1 (1.4)	2.0 (1.1)	2.2 (1.2)	1.8 (1.1)
Active metals interaction type	Based on XRD	Two separated metals (Pd, Cu)	Two separated metals (Pd, Cu)	Cu incorporated into the Pd lattice	Pd/Cu alloy + Pd
Pd particle size, nm (dispersion, %)		12.8 (8.7)	13.4 (8.3)	17.6 (6.3)	7.3 (15.2)
Cu particle size, nm (dispersion, %)		7.3 (14.2)	5.5 (18.8)	–	–
Pd-Cu alloy particle size, nm (dispersion, %)		–	–	–	14.0 (7.7)
Pd:Cu atomic ratio in alloy (based on lattice parameter)		–	–	90.6 at.% Pd + 9.4 at.% Cu	50 at.% Pd + 50 at.% Cu

Table 2
Catalytic denitration experimental conditions.

Reaction temperature (°C)	25
Reaction pressure (bar)	1
Initial NO_3^- concentration (ppm)	100
Catalyst weight (mg)	300
Water model system volume (ml)	700
Hydrogen flow rate (ml/min)	110
H_2/CO_2 flow rate ratio	1
pH	6
Stirring speed (rpm)	650

3. Results and discussion

3.1. Characterization of Pd-Cu/CNT catalysts

The morphology and size of bimetallic Pd-Cu and monometallic nanoparticles deposited on the carbon nanotubes were investigated by TEM, and representative images accompanied by corresponding histograms of metal particle size distribution are shown in Fig. 1. The microscopy images show the presence of well-defined nanoparticles, predominantly of round shape, dispersed on the external surface of nanotubes. Unsupported standalone particles were not observed in any of the catalysts examined. As can be seen from Fig. 1a–d, the Pd-Cu active phase in the Pd-Cu/CNT_{ACo} catalyst sample exhibits a more homogeneous distribution and a higher concentration of nanoparticles, compared to other catalysts. According to the corresponding histograms, all samples can be characterized by metal particle size distribution in the range of 2–30 nm, with a profile maximum at around 14, 15, 20 and 13 nm for the Pd-Cu/CNT_{ACo}, Pd-Cu/CNT_{MCo}, Pd-Cu/CNT_{AMo} and Pd-Cu/CNT_{MMo} samples respectively (Table 1). Furthermore, the TEM images of the Pd-Cu/CNT_{ACo} and Pd-Cu/CNT_{MCo} samples (Fig. 1a and b) reveal the existence of a certain proportion of smaller diameter nanoparticles, while the majority of large ones display a characteristic shape with clearly visible edges and terraces (marked by arrows). In the case of the Pd-Cu/CNT_{AMo} and Pd-Cu/CNT_{MMo} catalyst samples, a slight broadening of the particle size distribution occurs, relative to the previously mentioned catalysts. As well as having the smallest average metal particle diameter, the Pd-Cu/CNT_{MMo} catalyst sample differs from the others in its heterogeneous metal distribution – it being only a partial covering of the nanotube's external surface.

Fig. 2 shows the XRD patterns of the Pd-Cu/CNT catalyst samples examined, displaying characteristic peaks for Pd and/or Cu, both with a face-centered cubic structure, as well as characteristic CNT patterns. In the case the of Pd-Cu/CNT_{ACo} and Pd-Cu/CNT_{MCo} catalyst samples, Pd diffraction lines appear at 2Θ values of 39.9° (111), 46.4° (200) and 67.7° (220), having a cubic lattice parameter of 0.391 nm (COD database code: 1011110, Reference code 96-101-1111). The peaks located at 2Θ values of 42.9° (111), 50.0° (200) and 73.4° (220) can be attributed to the metallic copper (COD database code: 1011110, Reference code 96-901-3018). Since no shifting of these signals was noticed, it can be suggested that the Pd-Cu/CNT_{ACo} and Pd-Cu/CNT_{MCo} catalyst samples consist of individual monometallic nanoparticles and/or bimetallic ones with predominant monometallic phases of either Pd or Cu. The average crystallite sizes of Pd and Cu were 12.8 nm and 7.3 nm, respectively, for the Pd-Cu/CNT_{ACo} catalyst, while the Pd-Cu/CNT_{MCo} sample is characterized by slightly larger Pd (13.4 nm) and smaller Cu (5.5 nm) crystals (Table 1). The XRD pattern of the Pd-Cu/CNT_{AMo} catalyst reveals the existence of three peaks shifted 0.3° to higher values than those characteristic of Pd, with an average nanoparticle size of 17.6 nm. Specific Cu phase reflections were not detected, and so the shifted Pd reflections might be attributed to lattice contraction caused by Cu atoms being incorporated into the framework of Pd particles, to produce Pd-Cu ensembles [12]. The value determined for the Pd lattice parameter (0.388 nm) is smaller than the theoretical one (COD database code: 1011110, Reference code 96-101-1111), which supports the previous assumption. The phenomenon of chemically disordered nanoalloy formation can be explained by the Hume-Rothery rule [30,31], which posits the possibility of complete or partial solubility for two metals having similar crystal structures, identical valences and with a relative difference of less than 15% in their atomic radii. This is precisely the case for Pd and Cu with atomic radii of 0.137 nm [32] and 0.128 nm [33], respectively. This permits the Cu atoms to penetrate the Pd lattice, and this reduces the lattice symmetry. Even though the applied Pd/Cu loading should guarantee almost equal Pd:Cu atomic ratios in all the catalyst samples, in the case of the Pd-Cu/CNT_{AMo} sample, the average composition, derived from the calculated lattice parameter, by applying Vegard's law [34], was 90.6 at.% Pd and 9.4 at.% Cu (Table 1). This means the face-centered cubic crystal structure of the Pd was only partly decorated with Cu atoms, and suggests the presence of a certain amount of Cu as an amorphous phase. Based on the reflections at 2Θ values, of 42.7° (110), 62° (200) and 78.3° (211) (COD database code: 9008813, Reference code 96-900-8814), an ordered $Cu_{1.00}Pd_{1.00}$ nanoalloy was identified in the Pd-Cu/CNT_{MMo} catalyst, with an average particle size of 14.01 nm. Taking into account the applied calcination temperature, Pd-Cu alloying was quite feasible [35,36], and this was additionally comforted by the small extent of structural defects in the particular CNTs used as support for this catalyst (see Chapter 2.1) [5]. Next to the alloy, an individual Pd metallic phase was also recognized in the form of small nanoparticles (average diameter 7.3 nm) in the same sample (Table 1).

The results of Raman analysis of the Pd-Cu/CNTs catalysts, presented in Table 3 as net Raman parameter differences relative to the equivalent nanotubes [26], testify to the quality changes caused by the introduction of the Pd-Cu nanoparticles. Namely, changes in the ratios of I_D/I_G (density of defects), I_{2D}/I_G (crystallinity degree), as well as $I_{2D}/$

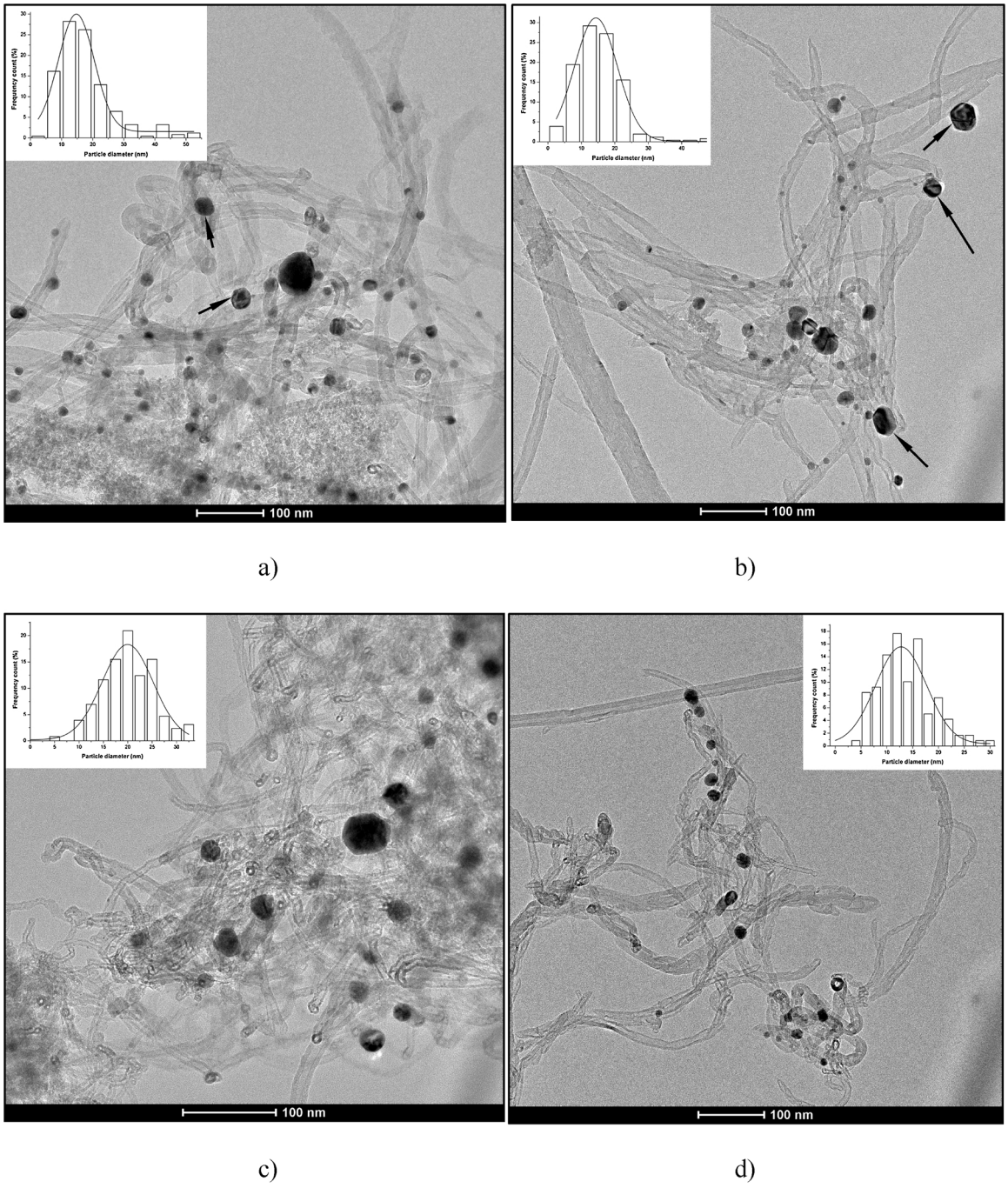

Fig. 1. TEM images (with the corresponding particle size histograms) of Pd-Cu nanoparticles in catalyst samples: a) Pd-Cu/CNT_{ACo}; b) Pd-Cu/CNT_{MCo}; c) Pd-Cu/CNT_{AMo} and d) Pd-Cu/CNT_{MMo}.

I_D (total structural quality) are undoubtedly the consequence of nanoparticle attachment to defect sites, on or within MWCNT surfaces [37]. Thus, the Pd-Cu/CNT_{MMo} catalyst shows the least amount of structural change, due to the high quality of the related CNT support exhibited as its lowest defect density (Table 1) [26]. Since surface defects have been considered as the main anchoring sites for metal nanoparticles [5,38], it can be assumed that the process of catalyst active-site genesis and evolution was preceded by the metals' increased mobility over the CNT surface. Subsequently, weak metal-support interaction has led to the alloy formation and the heterogeneous distribution of the nanoparticles (as confirmed by XRD and TEM), without any significant deterioration in the nanotube structure. On the other hand, the active phase incorporation process had the greatest impact on CNT quality during the Pd-Cu/CNT_{AMo} catalyst preparation. As confirmed by XRD and TEM, this sample contains the largest metal crystallites, probably built up from smaller species, susceptible to agglomeration because of the inadequate anchoring offered by the few defect sites in the related CNTs. In the growing process, the metal particles finally reach a size where Pd-C interaction is intensified, causing the prevalent structural changes in return. This fact is supported by the additional peak in the Raman spectra of the same Pd-Cu/CNT_{AMo} sample, located at 633 cm^{-1}, which is caused by Pd–C bond vibrations on the surface of the CNTs [39] (Fig. 3). For the other two samples, Pd-Cu/CNT_{ACo} and Pd-Cu/CNT_{MCo}, a moderate deterioration of the CNT network has occurred. As in the previous case, this is also governed, to some extent, by the size of the metal nanoparticles formed (especially the fraction of larger ones) and

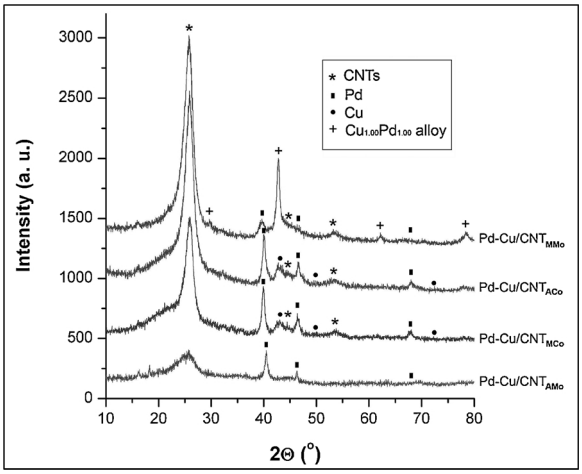

Fig. 2. The XRD patterns of examined Pd-Cu catalysts.

Table 3
Changes in Raman quality indicators for the Pd-Cu/CNT catalysts examined, upon Pd-Cu active phase introduction on the corresponding CNTs.

Sample				
Raman indicator changes	Pd-Cu/ CNT_{ACo}	Pd-Cu/ CNT_{MCo}	Pd-Cu/ CNT_{AMo}	Pd-Cu/ CNT_{MMo}
I_D/I_G increase	0.10	0.11	0.32	0.05
I_{2D}/I_G decrease	0.05	0.05	0.12	0.02
I_{2D}/I_D decrease	0.07	0.07	0.13	0.05

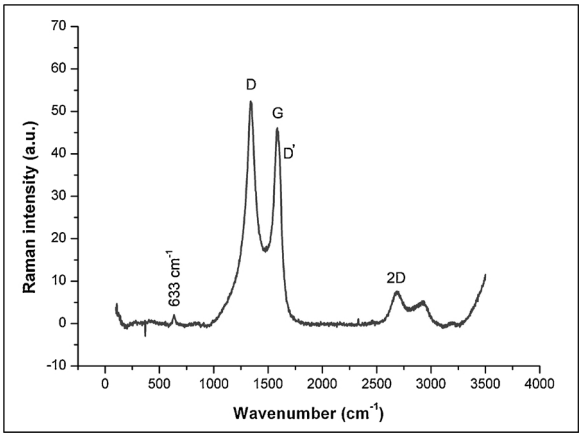

Fig. 3. Raman spectra of Pd-Cu/CNT_{AMo} catalyst.

their distribution over the CNT surface. In general, it can be assumed that the size of metal crystallites is increased by the decrease of defect site population on the CNTs, until their reduced amount enables the formation of an ordered nanoalloy. In the particular case of Pd-Cu/CNT_{MMo} sample, characterized by the weakest metal-support interaction among the synthesized catalysts, the increased mobility and susceptibility of both metals towards the formation of ordered $Cu_{1.00}Pd_{1.00}$ nanoalloy have initiated the redistribution of the active phase. Consequently, the resulting size of the alloy nanoparticles, grown next to the Pd individual metal crystallites, does not follow the trend governed by the extent of structural defects in the CNTs. Considering the pristine CNTs, a certain low level of structural defects can be designated as the critical one in terms of the specific (atypical) behavior of Pd-Cu active phase, affecting the size and composition of the formed metal crystallites.

3.2. Catalytic tests

Prior to catalytic examinations, all the synthesized Pd-Cu/CNT catalysts were checked for nitrate reduction by performing blank tests without H_2 as a reducing agent. The absence of products from both steps of the consecutive reaction proved that there was no reduction capacity.

The nitrate reduction activity of the catalysts tested is expressed as the remaining content of nitrate ions (ppm) in the system, as a function of reaction time. The proportion of nitrate ion conversion was calculated from the following expression:

$$X(NO_3^-) = \frac{n_i(NO_3^-) - n(NO_3^-)}{n_i(NO_3^-)} \cdot 100(\%) \quad (1)$$

where $n_i(NO_3^-)$ is the initial amount of nitrate ions (mmol) present in the system and $n(NO_3^-)$ is the amount of nitrate ions (mmol) present at time t.

The selectivity of the catalysts (%) was determined using the final quantities (mmol) of resulting nitrogen, as the desired product, nitrite ions as an intermediate product, and ammonium ions as an undesired product, at the end of the denitration reaction. The following expressions were employed for the calculation:

$$S(N_2) = \frac{2n(N_2)}{n_i(NO_3^-) - n(NO_3^-)} \cdot 100(\%) \quad (2)$$

$$S(NO_2^-) = \frac{n(NO_2^-)}{n_i(NO_3^-) - n(NO_3^-)} \cdot 100(\%) \quad (3)$$

$$S(NH_4^+) = \frac{n(NH_4^+)}{n_i(NO_3^-) - n(NO_3^-)} \cdot 100\,(\%) \quad (4)$$

where $n_i(NO_3^-)$ (mmol) and $n(NO_3^-)$ (mmol) have the same meaning as in Eq. (1), and $n(N_2)$ (mmol), $n(NO_2^-)$ (mmol) and $n(NH_4^+)$ (mmol) are the amounts of the respective species at time t. The quantity of nitrogen was determined as the difference between the total number of converted nitrate ions and the sum total of the resulting ammonia and nitrite ions assuming the corresponding stoichiometric ratio. The calculation assumes no NO_X formation other than NO_2^-. Catalytic performances, presented as individual concentration values with time-on-stream, are shown in Fig. 4, and values for nitrate conversion and appropriate selectivities at the end of the reaction are summarized in Table 4. TOF values were calculated based on dispersion results from TEM and according to the following expression:

$$TOF = \frac{n_i(NO_3^-)/t \cdot X(NO_3^-) \cdot M_{active\ metal}}{m_{catalyst} \cdot w_{active\ phase} \cdot dispersion(\%)}\ (\mathrm{min}^{-1}) \quad (5)$$

where $n_i(NO_3^-)$ (mmol) has the same meaning as in Eq. (1), t (min) is the total reaction time (240 min), $X(NO_3^-)$ (%) is the nitrate conversion at the end of the reaction, $M_{active\ metal}$ (g/mmol) is the molar mass of the catalyst active phase, $m_{catalyst}$ is the catalyst weight (g), while the $w_{active\ phase}$ is the catalyst active phase weight fraction.

According to the results presented in Fig. 4a, all four catalysts showed satisfactory activity for the chosen reaction time window, as concentrations of nitrate ions were below 50 ppm, the limit defined by the European Commission drinking water regulations. On the other hand, all ammonium values exceeded the maximum allowable concentration (0.5 ppm). The nitrite values obtained were at an acceptable level (< 0.5 ppm) for all tested catalysts. The data given in Table 4 shows that, based on an offset nitrate conversion degree of 60%, the four catalysts examined can be divided into two groups on the basis of their performance. That is to say, the catalyst samples with CNT supports having a higher proportion of lattice defects (Pd-Cu/CNT_{ACo} and Pd-Cu/CNT_{MCo}), show conversion levels up to 60%, while the catalysts prepared on CNT supports having no lattice defects or only a small proportion of lattice defects (Pd-Cu/CNT_{AMo} and Pd-Cu/CNT_{MMo}) show substantially higher nitrate conversion, around 80% and above. The

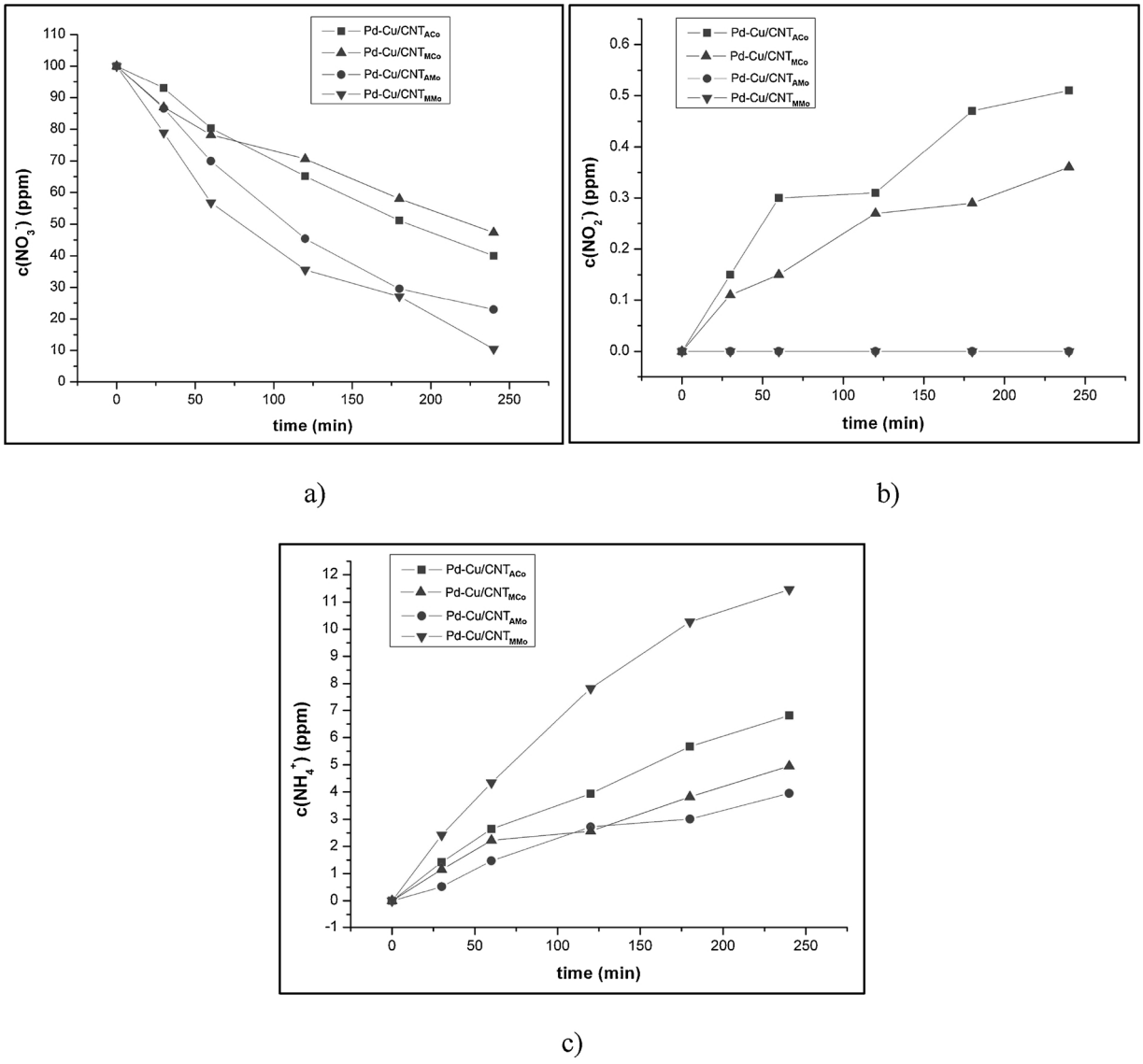

Fig. 4. Concentrations of a) nitrate; b) nitrite and c) ammonium ions as a function of reaction time during nitrate reduction in the presence of the examined Pd-Cu/CNTs catalysts.

Table 4
Values for nitrate conversion - X(NO_3^-), TOF, and nitrite, nitrogen and ammonium selectivities - S(NO_2^-), S(N_2), S(NH_4^+) at the end of the reaction, for the different Pd-Cu/CNT catalysts.

Sample				
t = 240 min	Pd-Cu/CNT$_{ACo}$	Pd-Cu/CNT$_{MCo}$	Pd-Cu/CNT$_{AMo}$	Pd-Cu/CNT$_{MMo}$
X(NO_3^-) (%)	60.0	55.6	79.7	89.5
TOF (min^{-1})	0.55	0.54	1.04	0.76
S(NO_2^-) (%)	1.1	0.9	0	0
S(N_2) (%)	59.9	66.7	82.3	55.8
S(NH_4^+) (%)	39.0	32.3	17.7	44.2

high activity of the former may be attributed to a beneficial arrangement in the Pd-Cu active phase, i.e. close contact between Pd and Cu, as in an alloy. According to several authors, the presence of bimetallic Pd-Cu entities is necessary for the first step of the denitration reaction (reduction of nitrate to nitrite), the two metals having distinct roles: Pd being responsible for hydrogen chemisorption and its spillover to copper, which in return reduces nitrate to nitrite [13,17,18]. The substantially higher activity found in this investigation in the case of both samples showing either unordered (Pd-Cu/CNT$_{AMo}$) or ordered (Pd-Cu/CNT$_{MMo}$) alloy, suggests that, although forming a composite, the Pd and Cu did not lose their basic individual properties for the reaction. The presence of the Pd-Cu alloy and its influence on catalyst activity have been discussed in the literature as a possible double-sided effect, having a beneficial aspect in terms of creating intimate contact between the Pd and Cu, and a limiting one, related to the decrease in metal surface causing the catalytic activity drop. The prevailing effect mostly depends on the catalyst reduction temperature, as well as the individual metal loadings [36]. Therefore, the lower denitration activity of those Pd-Cu/CNT catalysts originating from low quality CNT supports (Pd-Cu/CNT$_{ACo}$ and Pd-Cu/CNT$_{MCo}$) is due to lack of Pd-Cu contact, which has been triggered by the different "sticking" abilities of these metals to many of the defect sites on particular CNT surfaces. As a consequence, the Pd crystallite is of considerable size and the Cu is too far away (Table 1). In these circumstances the amount of H_2 adsorbed by the Pd and its availability to the Cu, due to diffusion constraints, have to be considered. Thus, the size of the Pd crystallite, both as an individual metal and in the alloy, appear to be of crucial importance for the

catalyst activity, and this is a function of the defect site population on the CNT support. Relatively high NO_3^- conversion in the case of the Pd-Cu/CNT_{AMo} catalyst sample (Table 4) shows that a suitable Cu position is beneficial for the reaction, although unproportional Pd and Cu atomic distribution occurs, and the majority of the copper is probably amorphous. However, the highest level of activity is found when the particle size and Pd and Cu atom distribution are optimal, as in the Pd-Cu/CNT_{MMo} catalyst sample (Table 4).

These results are in line with the TOF values presented in Table 4. The closeness of the TOF values obtained for the two high CNT-defect-originated catalyst samples (Pd-Cu/CNT_{ACo} and Pd-Cu/CNT_{MCo}) indicate active sites with the same potential for nitrate conversion. In contrast, in the catalyst samples originating from the CNTs with low levels of disorder (Pd-Cu/CNT_{AMo} and Pd-Cu/CNT_{MMo}) the active sites of the Pd-Cu/CNT_{AMo} sample, showing the highest TOF activity, result from unordered Pd-Cu alloy. As confirmed by TEM and XRD, the considerably higher particle size in this sample (Table 1) consists predominantly of high surface area palladium, only decorated with Cu atoms on its surface, enabling superior H_2 chemisorption and consequent spillover. This active site model is sustained by the lower surface energy of Cu relative to Pd [40], favoring Cu segregation on a Pd surface. On the other hand, in the case of the Pd-Cu/CNT_{MMo} sample, characterised by smaller particles of ordered Pd-Cu alloy, both H_2 chemisorption and spillover may be limited, due to the lack of a minimum number of gathered Pd atoms and/or its different electron perimeter, i.e. assemble effect and/or ligand effect [41]. However, the TOF values for all four samples presented in Table 4 are on the same scale as TOF values for catalysts with the same Pd-Cu active phase supported on active carbon, performing in the range 0.1–1.5 min^{-1} depending on the catalyst preparation method [42].

A close look at Fig. 4 and Table 4 may encourage skepticism with regard to the accepted mechanism of the denitration reaction. This is because both Pd-Cu/CNT catalysts prepared on ordered CNT structures, and displaying the highest levels of activity, show no traces of nitrite, while their lower activity counterparts present another surprising feature, i.e. NO_2^- profiles untypical for the consecutive reaction. It seems that these two extreme behaviors are due to the different kinetics of the two reaction steps occurring on the two groups of catalysts, which differ in many aspects of their active phase properties. The absence of NO_2^- does not exclude the reaction route comprising NO_3^- reduction to NO_2^- and such a case has been reported in the literature [29,42,43]. This can be explained by the second reaction step of NO_2^- reduction to either N_2 or NH_3 being much faster than the first reaction step of nitrate to nitrite conversion. Likewise, the absence of NO_2^- in the profile maximum from Figure 4b, for the Pd-Cu/CNT_{ACo} and Pd-Cu/CNT_{MCo} samples, suggests the second reaction step is always slower. This is in contrast to the expected kinetic rebound, which should happen because of the gradual nitrate concentration decrease over time (Figure 4a), and which should be followed by a takeover by the second reaction step. An explanation for the atypical kinetics observed might be found in the position of the Pd, which is the active phase for both second step reaction pathways, relative to the Cu. The close Pd-Cu proximity (like that of an alloy), in the Pd-Cu/CNT_{AMo} and Pd-Cu/CNT_{MMo} samples (Table 1), enables the formation of NO_2^- and its instant reduction, at the same particle, to either N_2 or NH_3. In contrast, diffusion constraints limit NO_2^- movement from the place of formation to the next Pd particle and make nitrite ions visible, as the first reaction step product. This is exactly what happened when the Pd-Cu/CNT_{ACo} and Pd-Cu/CNT_{MCo} catalyst samples were applied.

As seen from Table 4, the Pd-Cu/CNT_{MMo} sample stands out as the one with the highest undesired NH_3 selectivity. The occurrence of an alloy and its influence on the further course of the denitration reaction has been noted in the literature. It is suggested that selectivity can differ, depending on alloy composition and atom arrangement [35,44,45]. According to Salomé et al. [46], the existence of an alloy in a Pd-Cu catalyst composition may be responsible for low selectivity to nitrogen. However, results from the present investigation show the alloyed active phase as having the highest selectivity to N_2 (Pd-Cu/CNT_{AMo}, Table 4), and demand a different explanation. High undesired selectivity to NH_3 has been discussed in the literature in terms of Pd facet dilution by Cu atoms, leading to an increment in the number of isolated Pd atoms, which favor ammonia formation [36,47]. This is in line with findings that individual small Pd particles, with active centers prevailing on their edges and corners, are responsible for the deep hydrogenation of nitrite ions and the creation of ammonium [47]. The highest selectivity to NH_3 in the case of the Pd-Cu/CNT_{MMo} catalyst sample is a classic example of structure sensitivity effect, portrayed as a reaction rate increase following a catalyst active phase particle size downsizing – an “antipathetic reaction” [48,49]. That is to say, the highlighted Pd-Cu/CNT_{MMo} sample selectivity to ammonia is the result of small Pd particles (7.3 nm, Table 1), and a higher percentage of Pd atoms sitting on particle corners and edges than is the case with larger Pd particles. Moreover, the sequence of catalyst selectivity to N_2: Pd-Cu/CNT_{MMo} < Pd-Cu/CNT_{ACo} < Pd-Cu/CNT_{MCo} < Pd-Cu/CNT_{AMo}, follows the same sequence of increasing Pd particle size (nm) for the related catalysts: 7.3 < 12.8 < 13.4 < 17.6. The highest Pd-Cu/CNT_{AMo} selectivity to nitrogen might be additionally promoted by the position of Cu atoms when they are incorporated into the Pd lattice. The tendency of Cu atoms to be positioned primarily at low coordinated Pd particles sites has been noted previously [50]. Large Pd particles that are not favored for NH_3 production *per se*, are additionally favored by Cu blocking low coordinated Pd centers, i.e. the corners and edges responsible for NH_3 formation [47], resulting in the advantageous selectivity of the Pd-Cu/CNT_{AMo} sample to nitrogen.

4. Conclusions

Four Pd-Cu/CNT denitration catalysts were synthesized by Pd-Cu supporting on multiwalled carbon nanotubes (MWCNTs) of different structural quality, induced by their grown catalysts. The MWCNTs were not chemically modified in terms of attaching additional functional groups to their surface, and therefore might be considered as relatively inert towards decoration by metal nanoparticles, with only low active phase dispersion expected. However, different levels of structural defects in the MWCNTs was found to dictate the size and composition of the Pd-Cu active phase. CNTs having high levels of structural defects triggered the formation of bimetallic particles characterized by a smaller Pd crystallite size and a distant Cu phase, with the Pd and Cu too far apart for high nitrate to nitrite reduction activity. Further increases in the structural quality of the CNTs, manifesting itself as fewer structural defects, led to the formation of Pd-Cu alloys, which, regardless of their different structures, were characterized by optimal Pd particle size and the necessary intimacy of Pd and Cu phases. Despite both alloyed Pd-Cu compositions’ high activities, they differ tremendously in selectivity to nitrogen, due to different particle sizes in the free Pd phase. Thus the highest selectivity to NH_3 was observed in the sample with the ordered Pd-Cu alloy, which also had very small free Pd particles, which were responsible for nitrite to ammonia reaction. Both high denitration activity and selectivity to nitrogen were observed in the case of the sample with the unordered Pd-Cu alloy, which had Pd particles enriched by a very small number of Cu atoms positioned on edges and corners. Such particle morphology additionally decreases the number of active sites potentially responsible for the unwanted structure sensitive nitrite to ammonia reaction.

Acknowledgement

Financial support of the Serbian Ministry of Education, Science and Technological Development [grant number 172059] is highly appreciated. Ákos Kukovecz is grateful for funding by the NKFIH (OTKA) K112531 grant. This collaborative research was partially supported by the “Széchenyi 2020” program in the framework of GINOP-2.3.2-15-

2016-00013 “Intelligent materials based on functional surfaces – from syntheses to applications” project.

References

[1] P.T. Anastas, J.C. Warner, Green Chemistry: Theory and Practice, Oxford University Press, New York, 1998.
[2] N. Karousis, G.-E. Tsotsou, F. Evangelista, P. Rudolf, N. Ragoussis, N. Tagmatarchis, J. Phys. Chem. C 112 (2008) 13463.
[3] T. Prasomsri, D. Shi, D.E. Resasco, Chem. Phys. Lett. 497 (2010) 103.
[4] J. Yang, W. Zhou, C.H. Cheng, J.Y. Lee, Z. Liu, J. Phys. Chem. B 107 (2003) 6292.
[5] P. Serp, M. Corrias, P. Kalck, Appl. Catal. A: Gen. 253 (2003) 337.
[6] A. Felten, J. Ghijsen, J.-J. Pireaux, W. Drube, R.L. Johnson, D. Liang, M. Hecq, G. Van Tendeloo, C. Bittencourt, Micron 40 (2009) 74.
[7] E. Unger, G.S. Duesberg, M. Liebau, A.P. Graham, R. Seidel, F. Kreupl, W. Hoenlein, Appl. Phys. A: Mater. Sci. Process. 77 (2003) 735.
[8] R.S. Oosthuizen, V.O. Nyamori, Platinum Metals Rev. 55 (2011) 154.
[9] http://ec.europa.eu/environment/water/water-drink/index_en.html.
[10] U.I. Matatov-Meytal, Ind. Eng. Chem. Res. 44 (2005) 9575.
[11] A.E. Palomares, J.G. Prato, F. Rey, A. Corma, J. Catal. 221 (2004) 62.
[12] F. Zhang, S. Miao, Y. Yang, X. Zhang, J. Chen, N. Guan, J. Phys. Chem. C 112 (2008) 7665.
[13] K.D. Vorlop, T. Tacke, Chem. Ing. Technol. 61 (1989) 836.
[14] L. Lemaignen, C. Tong, V. Begon, R. Burch, D. Chadwick, Catal. Today 75 (2002) 43.
[15] I. Mikami, Y. Sakamoto, Y. Yoshinaga, T. Okuhara, Appl. Catal. B: Environ. 44 (2003) 79.
[16] A. Pintar, J. Batista, J. Levec, T. Kajiuchi, Appl. Catal. B: Environ. 11 (1996) 81.
[17] F. Epron, F. Gauthard, C. Pineda, J. Barbier, J. Catal. 198 (2001) 309.
[18] N. Barrabés, J. Just, A. Dafinov, F. Medina, J.L.G. Fierro, J.E. Sueiras, P. Salagre, Y. Cesteros, Appl. Catal. B: Environ. 62 (2006) 77.
[19] A. Miyazaki, K. Matsuda, F. Papa, M. Scurtu, C. Negrila, G. Dobrescu, I. Balint, Catal. Sci. Technol. 5 (2015) 492.
[20] F. Papa, I. Balint, C. Negrila, E.-A. Olaru, I. Zgura, C. Bradu, Ind. Eng. Chem. Res. 53 (2014) 19094.
[21] S. Panić, Á. Kukovecz, G. Boskovic, Appl. Catal. B: Environ. 225 (2018) 207.
[22] J. Batista, A. Pintar, D. Mandrino, M. Jenko, V. Martin, Appl. Catal. A: Gen. 206 (2001) 113.
[23] C.M. Mendez, H. Olivero, D.E. Damiani, M.A. Volpe, Appl. Catal. B: Environ. 84 (2008) 156.
[24] O.S.G.P. Soares, J.J.M. Órfão, M.F.R. Pereira, Ind. Eng. Chem. Res. 49 (2010) 7183.
[25] O.S.G.P. Soares, J.J.M. Órfão, M.F.R. Pereira, Catal. Lett. 139 (2010) 97.
[26] S. Panić, B. Bajac, S. Rakić, Á. Kukovecz, Z. Kónya, V. Srdić, G. Boskovic, React. Kinet. Mech. Cat. 122 (2017) 775.
[27] S. Ratkovic, Dj. Vujicic, E. Kiss, G. Boskovic, O. Geszti, Mat. Chem. Phys. 129 (2011) 398.
[28] S. Panic, D. Rakic, V. Guzsvány, E. Kiss, G. Boskovic, Z. Kónya, Á. Kukovecz, Chemosphere 141 (2015) 87.
[29] G. Boskovic, M. Kovacevic, E. Kiss, J. Radnik, M. Pohl, M. Schneider, U. Bentrup, A. Bruckner, Int. J. Environ. Sci. Technol. 9 (2012) 235.
[30] Hume-Rothery Rules, Van Nostrand’s Scientific Encyclopedia, (2005).
[31] A.-P. Tsai, J. Non-Cryst. Solids 334 (2004) 317.
[32] L. Zhang, J. Zhang, Z. Jiang, S. Xie, M. Jin, X. Han, Q. Kuang, Z. Xie, L. Zheng, J. Mater. Chem. 21 (2011) 9620.
[33] V.A. Kukareko, A.G. Kononov, Phys. Solid State 51 (2009) 286.
[34] L. Vegard, Z. Phys. 5 (1921) 17.
[35] O.S.G.P. Soares, J.J.M. Órfão, J. Ruiz-Martínez, J. Silvestre-Albero, A. Sepúlveda-Escribano, M.F.R. Pereira, Chem. Eng. J. 165 (2010) 78.
[36] J. Sá, S. Gross, H. Vinek, Appl. Catal. A: Gen. 294 (2005) 226.
[37] M. Baro, P. Nayak, T.T. Baby, S. Ramaprabhu, J. Mater. Chem. A 1 (2013) 482.
[38] Z. Zhong, B. Liu, L. Sun, J. Ding, J. Lin, K.L. Tan, Chem. Phys. Lett. 362 (2002) 135.
[39] A.K. Mishra, S. Ramaprabhu, Chem. Eng. J. 187 (2012) 10.
[40] H.L. Skriver, N.M. Rosengaard, Phys. Rev. B 46 (1992) 7157.
[41] W.M.H. Sachtler, G. Ertl, H. Knözinger, J. Weitkamp (Eds.), Handbook of Heterogeneous Catalysis, Vol. 3 VCH, Weinheim, 1997p. 1077.
[42] J. Trawczyński, P. Gheek, J. Okal, M. Zawadzki, M.J. Ilan Gomez, Appl. Catal. A: Gen. 409-410 (2011) 39.
[43] I. Dodouche, D.P. Barbosa, M.C. Rangel, F. Epron, Appl. Catal. B: Environ. 93 (2009) 50.
[44] J. Batista, A. Pintar, Dj. Mandrino, M. Jenko, V. Martin, Appl. Catal. A: Gen. 206 (2001) 113.
[45] F. Deganello, L.F. Liotta, A. Macaluso, A.M. Venezia, G. Deganello, Appl. Catal. B: Environ. 24 (2000) 265.
[46] O.S.G.P. Soares, J.J.M. Órfão, M.F.R. Pereira, Appl. Catal. B: Environ. 91 (2009) 441.
[47] Y. Yoshinaga, T. Akita, I. Mikami, T. Okuhara, J. Catal. 207 (2002) 37.
[48] M. Boudart, Adv. Catal. 20 (1969) 152.
[49] M. Che, C.O. Bennett, Adv. Catal. 36 (1989) 55.
[50] R. Mélendrez, G. Del Angel, V. Bertin, M.A. Valenzuela, J. Barbier, J. Mol. Catal. A 157 (2000) 143.